

Synergistic Combination of Crosslinked Polymer and Concentrated Ionic Liquid for Electrolytes with High Stability in Solid-State Lithium Metal Batteries

Mingjie Zhang^{a,c}, Faezeh Makhlooghi azad^{c*}, Urbi Pal^c, Mahin Maleki^c, Shinji Kondou^c
Giuseppe A. Elia^{a,b}, Claudio Gerbaldi^{a,b*}, and Maria Forsyth^c

^aGAME Lab, Department of Applied Science and Technology (DISAT), Politecnico di Torino, Corso Duca degli Abruzzi 24, 10129, Torino, Italy

^bNational Reference Center for Electrochemical Energy Storage (GISEL) - INSTM, Via G. Giusti 9, 50121, Firenze, Italy

^cInstitute for Frontier Materials (IFM), Deakin University, Burwood, Victoria 3125, Australia.

* f.makhlooghi azad@deakin.edu.au, claudio.gerbaldi@polito.it

Abstract

PEO-based solid polymer electrolytes (SPEs) are regarded as excellent candidates for solid-state lithium metal batteries (LMBs) due to their inherent safety advantages, processability, low cost and excellent Li ion solvation. However, they suffer from limited oxidation stability (up to 4 V vs. Li⁺/Li). In this study, a newly designed crosslinked polymer-in-concentrated ionic liquid (PCIL) SPE consisting of PEO, C₃mpyrFSI and LiFSI is developed. The adopted UV-crosslinking strategy synergistically reduces PEO crystallinity while increasing the amount of encompassed lithium salt and IL, and improves PEO oxidative stability, therefore leading to enhanced electrochemical performance. The physical and electrochemical properties of both linear and crosslinked SPEs are explored and compared. The designed crosslinked SPEs exhibited a promisingly high oxidative stability of 4.9V vs. Li⁺/Li and high ambient temperature ionic conductivity of 4×10^{-4} S cm⁻¹. Stable and reversible lithium plating/stripping is demonstrated in symmetrical Li||Li cells over hundreds of hours. High loading solid-state LFP||Li cells showed favourable cycling with over 90% capacity retention at 0.1C over 100 cycles at 50°C. High voltage solid-state LMO||Li cells exhibited promising cycling with 93% capacity retention at 0.2 C rate over 50 cycles at 50°C. Both cathodes utilized a high areal capacity of 1 mAh cm⁻². The synergistic combination of crosslinking and concentrated ionic liquid electrolyte to a robust SPE enables a new pathway for designing high-performing PEO-based SPEs for high energy density solid-state LMBs.

1. Introduction

The pursuit of advanced energy storage technologies has significantly featured the role of lithium metal batteries (LMBs) owing to their superior energy density and potential for enabling long-range electric vehicles. However, the widespread adoption of LMBs is hindered by safety concerns related to liquid electrolytes, which are prone to flammability and stability issues. This has promoted the exploration of solid electrolytes as a safer alternative. The pioneering work of Wright and Armand in 1970s ignited the interest and passion for research into solid polymer electrolytes (SPEs) for rechargeable solid-state batteries.^{1,2} Since then, polyethylene oxide (PEO) has become a frontrunner in SPEs due to its high safety, ease of processing, low cost, and good compatibility with lithium metal, making it attractive for integration into next-generation LMBs.^{3,4} High molecular weight PEO offers the benefits of preventing Li dendrite formation due to its superior mechanical properties and enhancing cycling stability compared to its lower molecular weight counterpart.⁵ However, ionic conductivity of PEO at room temperature is inadequate (up to 10^{-6} S cm⁻¹) because its semi-crystalline structure which hinders chain mobility, essential for ion transport, often requiring higher temperatures for effective application. Additionally, PEO-based solid polymer electrolytes (SPEs) are limited by a narrow electrochemical stability window (ESW < 4V vs. Li⁺/Li) due to the low oxidative stability of ether oxygen.^{1,4,5} These drawbacks considerably constrain their practical use in high voltage solid-state lithium metal batteries (LMBs). To overcome these issues, research has focused on modifying the PEO microstructure, including the addition of inorganic fillers,^{6–8} plasticizing ionic liquids,¹⁰ copolymerization,¹¹ and creating crosslinked PEO matrices.^{9,10}

Ionic liquid (IL)-based electrolytes have gained significant interest in recent years due to their superior properties, such as low vapor pressure, nonflammability, and outstanding thermal and chemical stability.¹¹ Shin et al. investigated the impact of C₃mpyrTFSI ionic liquid on the ionic conductivity of PEO-based ternary polymer electrolytes, and demonstrated that the inclusion of highly conductive room temperature ILs significantly enhances ionic conductivity, surpassing the limits previously observed in IL-free electrolytes.¹² Crosslinking, as a versatile polymerization technique, is often used to improve the mechanical property and hinder polymer crystallization of plasticized SPEs.^{10,13} Watanabe et al. first studied the crosslinked PEO-LiClO₄ systems which showed decreased PEO crystallinity by decreasing T_g from -22 to -30°C and enhanced ionic conductivity from 10^{-9} to 10^{-5} S cm⁻¹ at 30°C compared to linear PEO system (EO/Li mole ratio = 20).¹⁴ Joost et al. further explored ionic mobility in crosslinked PEO-based ternary SPE systems that incorporate C₄mpyrTFSI ionic liquid with relatively low concentration of LiTFSI (25 mol%), demonstrating a decrease of Li⁺-EO interactions in the ternary system due to the additional TFSI⁻ anions from ionic liquid that contributes to the high ionic conductivity.¹⁵ The crosslinking process, induced by UV irradiation, helps to form a stable network that enhances the mechanical integrity of the SPE while accommodating the beneficial properties of ILs. The effectiveness of UV-induced crosslinking in the development of polymer-plasticiser-salt ternary systems was further validated by other researchers.^{16,17}

In recent years, inspired by the concept of high concentrated electrolyte in traditional liquid electrolytes,^{18–20} there is growing interest in concentrated ionic liquid (CIL) electrolytes due to their advantageous properties such as expanded electrochemical stability window,²¹ high transference number,²² high rate capability,²³ and enhanced cycling stability.²⁴ Recent work from Pal et al. identified the use of ether-aided concentrated LiFSI-C₃mpyrFSI ionic liquid electrolyte as an effective approach to enhance ion transport, interfacial stability, and support fast charging.^{25–27} These desirable properties make them promising candidates to work with the crosslinking strategy for developing high-performance PEO-based SPEs. Thus, one

promising approach to form a robust PEO-based SPE is to combine crosslinking with the incorporation of CILs, which shows great potential in further suppressing PEO crystallinity, improving ionic conductivity, expanding electrochemical stability while maintaining safety and mechanical integrity.

In this work, we report a novel UV-crosslinked polymer-in-concentrated ionic liquid system (PCIL) based on PEO, lithium bis(fluorosulfonyl)imide (LiFSI) and N-propyl-N-methylpyrrolidinium bis(fluorosulfonyl)imide (C_3 mpyrFSI) ionic liquid (Li^+ :IL molar ratio = 1:1). By focusing on the enhancement of ion transport, electrochemical stability, and cell performance, we seek to tackle a critical gap in the current understanding of PEO-based SPEs. The obtained PCIL-SPEs achieved high ambient temperature ionic conductivity, wide electrochemical stability window, stable and reversible cycling toward Li metal electrodes and promising solid-state LMB performance. Thus, by incorporating concentrated ionic liquids with UV-crosslinking to form a robust SPE, we shed light on the potential of PEO-based SPEs to meet the rigorous demands of high-performing solid-state LMBs and pave the way for their practical application in future advanced energy storage systems.

2. Experimental Section

2.1 Materials

Poly(ethylene oxide) (PEO, M_w 5,000,000, Sigma-Aldrich) was subjected to vacuum drying at 50 °C for 24 hours before use. N-propyl-N-methylpyrrolidinium bis(fluorosulfonyl) imide (C_3 mpyrFSI, purity 99.5%, Solvionic) and lithium bis(fluorosulfonyl)imide (LiFSI, purity 99.9%, Nippon Shokubai) was subjected to vacuum drying at 50 °C for 48 hours before use. Benzophenone (BP) obtained from Sigma-Aldrich was utilized without further purification for the crosslinking process. Lithium iron phosphate (LFP) was purchased from Custom Cells with areal capacity of 1 mAh cm⁻² and active mass loading of ~ 6 mg cm⁻². Lithium manganese oxide (LMO) powder was provided by Calix Ltd. Carbon superP65 was obtained from Sigma Aldrich and polyvinylidene fluoride (PVDF) was ordered from Alfa Aesar (99.9% purity). Materials were stored in Ar-filled glove boxes before SPE preparation.

2.2 Solid Polymer Electrolyte Preparation

The polymer-in-concentrated ionic liquid SPEs (PCIL-SPEs) were prepared using a solvent casting technique within an Ar-filled glovebox. The preparation steps are shown in **Figure 1**. First, predetermined amounts of LiFSI salt and C_3 mpyrFSI IL (Li^+ :IL molar ratio = 1:1) were mixed and dissolved overnight at room temperature. Then the obtained solutions were mixed with various amount of PEO in acetonitrile with EO: Li^+ :IL molar ratios equal to 10:1:1. The obtained solutions were then cast into silicon moulds and rested for 48 hours to ensure slow evaporation of solvent. The obtained free-standing solid membranes were then sandwiched between two Mylar foils and hot-pressed (70°C, 2 MPa for 10 mins) to obtain homogenous membranes with a thickness of $150 \pm 10\mu m$. Crosslinked PCIL-SPEs were prepared by using benzophenone (BP, 5 wt% of PEO) as photo-initiator and crosslinked in a TBK 905 UV curing box (power 200W) for 3 mins right after hot-pressing. The prepared SPEs were then transferred to the Buchi oven for a secondary vacuum drying process (50°C for 24 h) before further characterization. All prepared SPEs were kept in argon-filled glovebox.

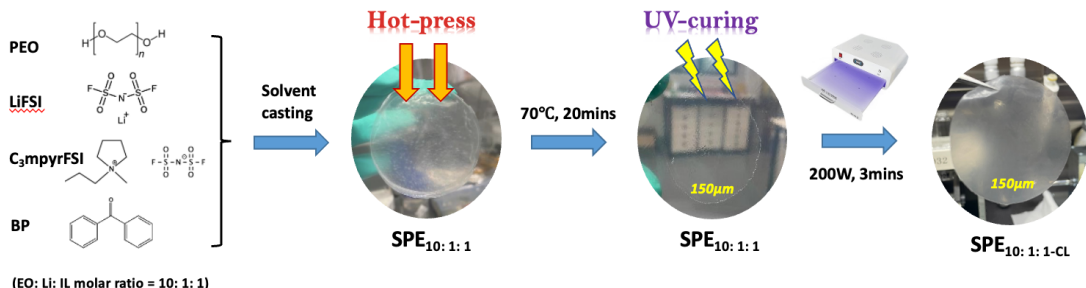


Figure 1. PCIL-SPEs (linear and crosslinked) prepared by solvent casting followed by hot-press and UV-crosslinking.

2.3 Characterization techniques

A Mettler Toledo Differential Scanning Calorimetry (DSC) instrument was used to study the phase behaviour of the designed SPEs. The measurements were performed over -120 – 80 °C at a heat/cooling rate of 10°C min⁻¹. Sample loading was kept approximately 10 mg.

Ionic conductivity (σ) of the designed SPEs was measured by electrochemical impedance spectroscopy (EIS) analysis (MTZ-35 impedance analyser, Biologic). The measurements were performed over the temperature range of 30–50 °C in frequency from 0.1 Hz to 1 MHz. A SS|PCIL-SPEs|SS (stainless-steel) coin cell configuration was used. The bulk resistance was calculated from the impedance curve at high frequency, and the ionic conductivity was calculated by the equation:

$$\sigma = \frac{l}{R_b \cdot A}$$

where σ is the ionic conductivity (S cm⁻¹), R_b is the bulk resistance (derived from the impedance curve), l is the membrane thickness and A is the area.

Raman spectra were obtained using a Renishaw Invia microscope with a laser generating 633 nm (red) light delivering 13.0 mW at the sample. The laser power was set to 10% with the exposure time of 60s and one accumulation. All measurements were done under room temperature in a sealed homebuilt sample holder with a quartz window in the range of 100 to 3200 cm⁻¹. Baseline corrections and normalization were applied to the spectra. The Voigt function was used to deconvolute bands into constituent peaks.

Thermal gravimetric analysis (TGA) was performed using a Mettler Toledo TGA STAR instrument to understand the thermal stability of the SPEs. with a sample loading of 10 mg. Mass loss was recorded over 30–600 °C with a 10 °C min⁻¹ heating rate under constant N₂ flow. Sample loading was kept approximately 10 mg.

Scanning electron microscope (SEM) analysis was carried out for the pristine SPEs as well as cycled cells. A coin cell disassembly unit (Hohsen) was used inside a glove-box to disassemble the cycled cells. The JSM-IT300 SEM from JEOL (Japan) was used to study the surface and cross-section morphology with a 10 kV acceleration voltage.

2.4 Electrode preparation, cell assembly and electrochemical measurements

The LMO electrode was prepared by mixing LMO powders, Super C65 and PVDF (80:10:10 wt.%) in NMP. The casting and drying methods for the LMO cathodes were as previously described.²⁸ The resulting LMO electrodes have a loading of 7 mg cm⁻² and an area capacity of 1 mA cm⁻². On the other hand, the LFP electrode from Custom Cells has a

similar areal capacity of 1 mA cm^{-2} with $\sim 6 \text{ mg cm}^{-2}$ active material loading. The electrodes were then cut into 8 mm diameter discs before coin cell assembly.

For all the battery measurements, lithium metal (100 μm , Gelon) was used as anode material. Battery cells were then assembled using a Li metal anode, a free-standing designed SPE membrane, and the prepared LFP/LMO cathodes.

Electrochemical measurements were performed using a multi-channel potentiostat VMP3 (BioLogic) with all measurements conducted in CR2032 coin cells (Hohsen Corp.). Linear sweep voltammetry (LSV) experiments were performed using a Li||SS (stainless steel) cell at 50 $^{\circ}\text{C}$. The scans ran from the open-circuit voltage (OCV) up to 6 V (vs. Li/Li $^{+}$) at a scan rate of 0.1 mV s $^{-1}$. The galvanostatic cycling for Li||Li, LFP||Li, and LMO||Li cells were also carried out. Cell cycling was performed at 50 $^{\circ}\text{C}$, with voltage limits set to 2.5-4 V vs. Li $^{+}$ /Li for LFP||Li cells and 3-4.3 V vs. Li $^{+}$ /Li for LMO||Li cells. Two formation cycles were used before long-term cycling unless mentioned otherwise. The reproducibility of the results has been checked by multiple tests.

3. Results and Discussion

3.1 Properties of designed PCIL-SPEs

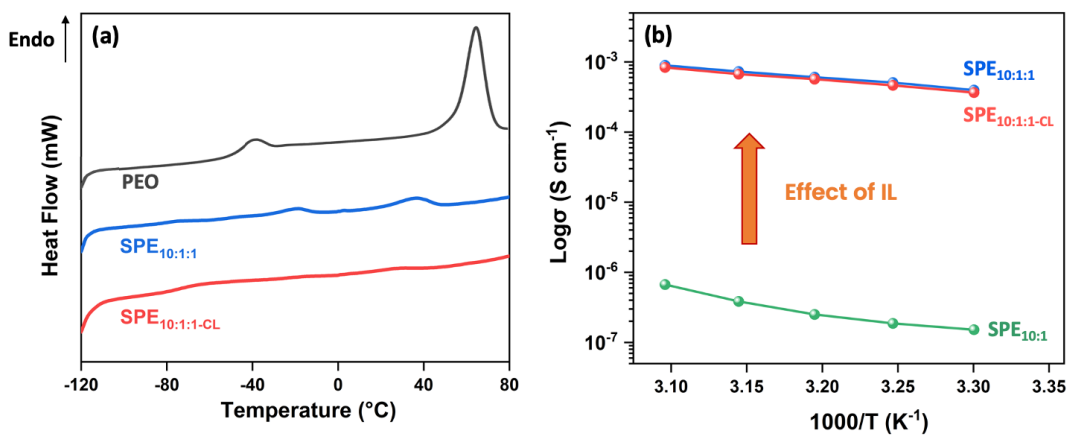


Figure 2. (a) Phase behaviour of crosslinked SPE_{10:1:1-CL} compared with linear SPE_{10:1:1} and pure PEO. (b) ionic conductivity of crosslinked SPE_{10:1:1-CL} compared with linear SPE_{10:1:1} and linear SPE_{10:1} without IL.

Both linear and crosslinked PCIL-SPEs were synthesized from homogeneous mixtures of PEO, LiFSI and C₃mpyrFSI (EO:Li:IL molar ratio=10:1:1) by solvent casting and UV-crosslinking processes, namely SPE_{10:1:1} and SPE_{10:1:1-CL} respectively (**Figure 1**). Thermal gravimetric analysis (TGA) of both SPE_{10:1:1} and SPE_{10:1:1-CL} confirms the thermal stability up to 220 $^{\circ}\text{C}$ which is sufficiently high for the safe operation of solid-state LMB (**Figure S1**, Support Information).

The effect of UV-crosslinking on the phase behaviour, ionic conductivity, and morphology of the prepared PCIL-SPEs are shown in **Figure 2** and **Figure S2**. As illustrated in **Figure 2a**, both the melting point and enthalpy decrease dramatically after introducing CIL (Li:IL molar ratio = 1:1) to PEO, with the melting transition temperature drops from 65 $^{\circ}\text{C}$ of pure PEO to 38 $^{\circ}\text{C}$ of SPE_{10:1:1}, and the Tg broadens significantly, suggesting a more complex heterogenous system.^{29,30} Notably, a small peak at approximately -20 $^{\circ}\text{C}$ appears in SPE_{10:1:1}, attributed to a phase transition in the C₃mpyrFSI/LiFSI mixture, suggesting limits in IL solubility and potential phase separation.^{31,32} Crosslinking SPE_{10:1:1} to create SPE_{10:1:1-CL} results in the disappearance of both the melting and phase transition peaks, with a new, pronounced Tg appearing at -74 $^{\circ}\text{C}$. This suggests that crosslinking leads to a highly

amorphous structure and enhances the uptake of IL in PEO matrix.¹⁰ In addition, the presence of a single Tg in the crosslinked materials indicates a good miscibility between IL and the PEO matrices.³³ To summarize, crosslinking effectively hinders crystallization of PEO and PEO-LiFSI complexes and increases the IL uptake in the crosslinked network, which is crucial for achieving high ionic conductivity due to the resulting high amorphicity of the SPEs.

Figure 2b illustrates the effect of IL content and UV-crosslinking on the ionic conductivity of the prepared SPEs. Compared to systems without IL (SPE_{10:1}), adding IL significantly increases the ionic conductivity, with more than three orders of magnitude improvement from $1.5 \times 10^{-7} \text{ S cm}^{-1}$ for IL-free SPE_{10:1} to $4 \times 10^{-4} \text{ S cm}^{-1}$ for SPE_{10:1:1} at 30°C as reported in our previous study,³⁰ suggesting the substantial role of IL in enhancing ionic conductivity. After crosslinking, SPE_{10:1:1-CL} shows a slight decrease in conductivity, consistent with an overall high salt content system.³⁴ Crosslinking generally increases the formation of amorphous phases that facilitate conductivity in systems with high polymer content.³⁵ However, it can also restrict polymer chain movement, hindering ion transport. This effect is particularly noticeable in systems with low polymer content that are already highly amorphous and conductive, such as SPE_{10:1:1}.³⁴ Overall, while crosslinking affects ionic conductivity by restricting chain mobility, its downside impact is mitigated by the reduced SPE crystallinity and increased IL uptake. Furthermore, the impact of crosslinking on ionic conductivity is much less pronounced compared to the influence of IL concentration.

The surface morphology of the prepared SPEs was characterized by SEM analysis as shown in **Figure S2**. Compared to SPE_{10:1:1}, the crosslinked SPE_{10:1:1-CL} shows a dense, smooth surface with a high degree of amorphous nature. The nonuniform and hardly homogeneous texture of SPE_{10:1:1} transformed into a finer wrinkled feature after crosslinking, which might be due to the increased encompassing of lithium salt and IL, leading to a more homogenous and mechanically robust network.^{13,36}

3.2 Raman Spectroscopy Analysis

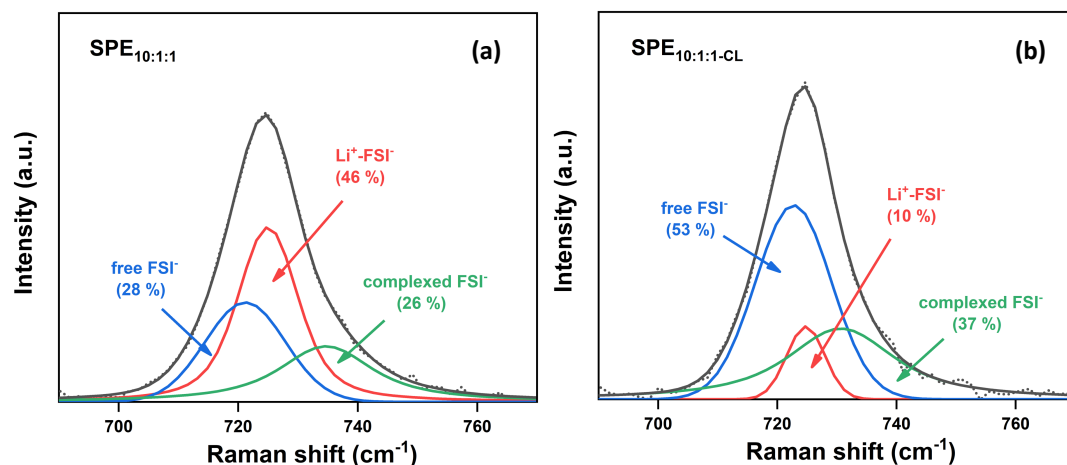


Figure 3. Raman spectra of -SNS stretching vibration mode of FSI⁻ anions in (a) linear SPE_{10:1:1} and (b) crosslinked SPE_{10:1:1-CL}. The spectra were deconvoluted to three FSI⁻ states, including free FSI⁻, Li⁺-FSI⁻ ion pairs, and complexed FSI⁻.

Raman spectroscopy was performed on linear SPE_{10:1:1} and crosslinked SPE_{10:1:1-CL} to investigate and reveal the effect of crosslinking on cation-anion interactions by identifying the states of FSI⁻ in the Raman shift between 700 and 800 cm⁻¹ (full Raman spectra is given in **Figure S3**, Supporting Information). The -SNS stretching mode of FSI⁻ in the PCIL-

SPEs was deconvoluted into three constituent peaks: free FSI⁻ at 721-723 cm⁻¹, Li⁺-FSI⁻ ion pairs at 725 cm⁻¹, and complexed FSI⁻ anions at 730-735 cm⁻¹ (aggregated ion clusters).³⁷ As shown in **Figure 3**, the SPE_{10:1:1} (Fig. 3a) has a low proportion of the free FSI⁻ state (28%) and a high proportion of Li⁺-FSI⁻ ion pairs (46%). In contrast, the crosslinked SPE_{10:1:1-CL} (Fig. 3b) is rich in free FSI⁻ anions (53%) and contains very low proportion of Li⁺-FSI⁻ ion pairs (10%), likely ascribed to the crosslinking of the EO chains that form a crosslinked network with high dissociation ability.³⁸ The resulting high solvation environment may lead to an increased Li⁺-EO coordination that can lower the highest occupied molecular orbital (HOMO) level of PEO and therefore benefit the electrochemical stability of the SPE.^{20,39} The SPE_{10:1:1-CL} also exhibited higher proportion of complexed FSI⁻ anions, indicating the presence of aggregated ion clusters. The crosslinked polymer network may have helped to segregate the large, aggregated domains into more uniformly distributed ion clusters to facilitate Li⁺ transport.³⁸ Therefore, we believe that crosslinking results in enhanced Li⁺ solvation and more uniformly distributed ion clusters which would account for the high ionic conductivity and the potential high electrochemical stability of the crosslinked SPE_{10:1:1-CL}.

3.4 Electrochemical characterisation

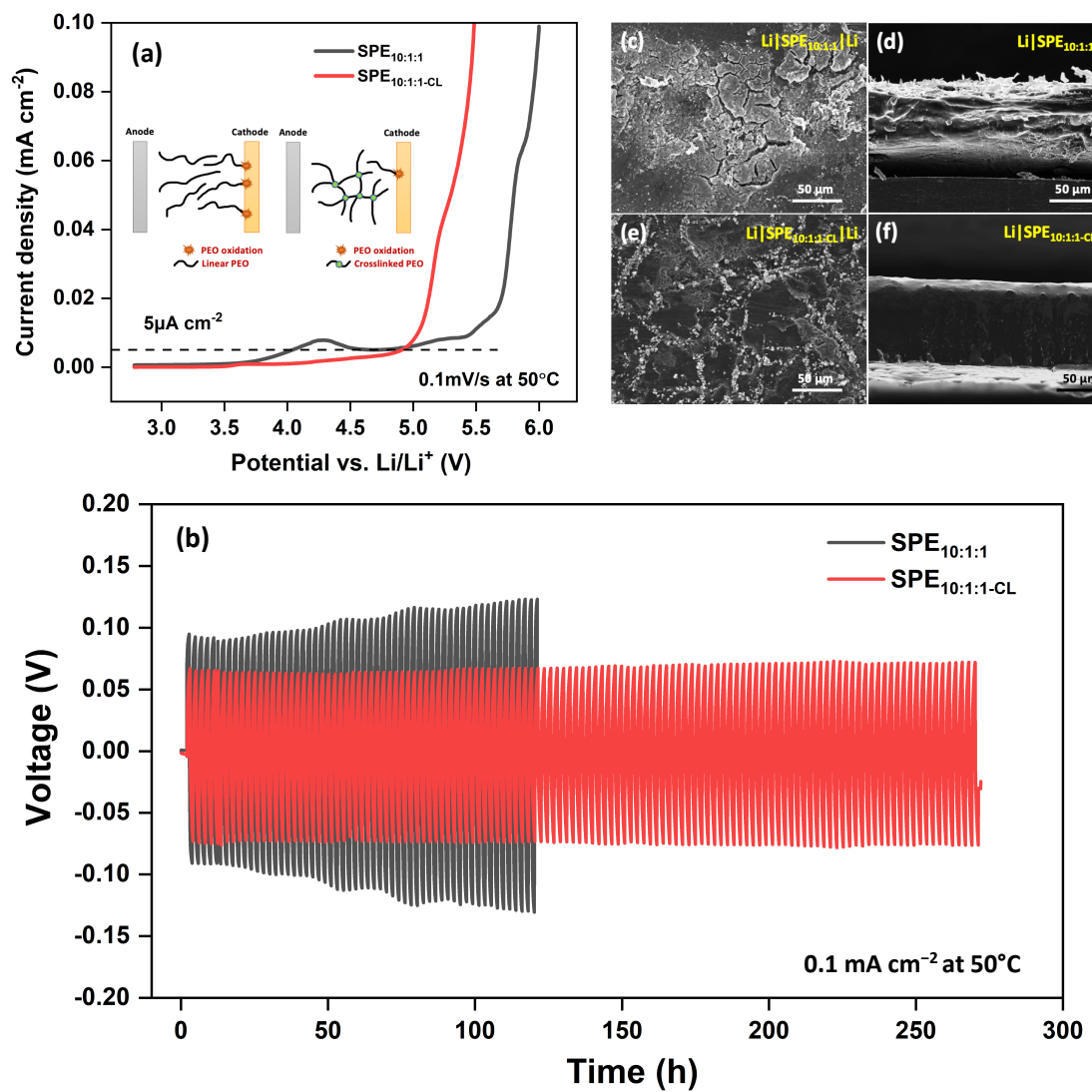


Figure 4. (a) Linear sweep voltammetry of $\text{SPE}_{10:1:1}$ and $\text{SPE}_{10:1:1-\text{CL}}$ in a $\text{Li}||\text{SS}$ cell with a scan rate of 0.1 mV s^{-1} at 50°C . (b) Voltage profiles of $\text{Li}|\text{SPE}_{10:1:1}|\text{Li}$ and $\text{Li}|\text{SPE}_{10:1:1-\text{CL}}|\text{Li}$ cells at 0.1 mA cm^{-2} . Surface (c, e) and Cross-section (d, f) SEM images of Li electrodes after cycling.

The electrochemical stability window (ESW) of the linear $\text{SPE}_{10:1:1}$ and crosslinked $\text{SPE}_{10:1:1-\text{CL}}$ was evaluated in a $\text{Li}||\text{SS}$ cell by LSV measurements. As shown in **Figure 4a**, the linear $\text{SPE}_{10:1:1}$ begins to oxidize slowly above 4V vs. Li^+/Li , a common behaviour in PEO-based SPEs. In contrast, the crosslinked $\text{SPE}_{10:1:1-\text{CL}}$ showed high electrochemical stability up to 4.9V vs. Li^+/Li ($5\mu\text{A cm}^{-2}$ current density was used as the cut-off of a current rise^{40,41}). This indicates its excellent oxidation stability and suitability for use with high-energy 4V -classs electrodes. The enhanced electrochemical stability of $\text{SPE}_{10:1:1-\text{CL}}$ can be attributed to its crosslinked network, which limits the mobility of linear EO chains and therefore reduces their likelihood of oxidation at the cathode surface as illustrated in the inserts in **Figure 4a**. Furthermore, the crosslinking changes the coordination environment enhancing more Li^+ -EO coordination and promoting the formation of FSI^- -rich ion clusters, as evidenced by Raman analysis. These coordinated ions and surrounding ion clusters likely form a protective layer that prevents further oxidation of EO, synergistically contributing to the enhanced oxidation stability.

The ability of the crosslinked $\text{SPE}_{10:1:1-\text{CL}}$ to support lithium plating-stripping at various current densities was assessed using $\text{Li}||\text{Li}$ symmetrical cells at 50°C , with current densities ranging from 0.05 up to 0.4 mA cm^{-2} . The cells showed overpotentials of 20 mV and 125 mV at 0.05 and 0.4 mA cm^{-2} respectively. As illustrated in **Figure S4**, the SPE can sustain plating-stripping polarization steps throughout the entire polarization period up to 0.4 mA cm^{-2} , demonstrating stable interfacial properties, thus compatibility with the lithium metal electrodes, and good cycling performance for a solid-state polymer electrolyte.

As shown in **Figure 4b**, the long-term cycling of the $\text{Li}|\text{SPE}_{10:1:1-\text{CL}}|\text{Li}$ cell cycled at 0.1 mA cm^{-2} for 1 hour polarisation demonstrated very stable performance, maintaining an overpotential of 60 mV over 130 cycles at 50°C , with no evidence of short circuit. This indicates that crosslinked $\text{SPE}_{10:1:1-\text{CL}}$ is highly compatible with the Li metal electrode. The interfacial resistance decreases after 130 cycles (shown in **Figure S5a**), suggesting the formation of an ion-conductive and stable SEI layer at the electrode/electrolyte interface. In contrast, the $\text{Li}|\text{SPE}_{10:1:1}|\text{Li}$ cell exhibits a steady increase in overpotential and a short circuit after just 60 cycles. The impedance spectra also showed an increase in interfacial resistance upon successive cycling as seen in **Figure S5b**.

The top- and cross-section SEM images of the Li electrodes from both cells after cycling ($\text{Li}|\text{SPE}_{10:1:1}|\text{Li}$ cell for 60 cycles, $\text{Li}|\text{SPE}_{10:1:1-\text{CL}}|\text{Li}$ cell for 130 cycles) are shown in **Figure 4c-f**. In the $\text{Li}|\text{SPE}_{10:1:1}|\text{Li}$ cell, the electrode surface displays large cracks and mossy Li formations (**Fig. 4c**), whereas the $\text{Li}|\text{SPE}_{10:1:1-\text{CL}}|\text{Li}$ cell shows a smooth and dense Li metal surface (**Fig. 4e**), indicating a uniform Li plating-stripping process. The cross-section images revealed a thick layer of dendritic/dead Li at the interface of the $\text{Li}|\text{SPE}_{10:1:1}|\text{Li}$ cell (**Fig. 4b**), in contrast to a dense and uniform interface observed in the $\text{Li}|\text{SPE}_{10:1:1-\text{CL}}|\text{Li}$ cell (**Fig. 4f**). This confirmed the formation of a smooth and compact interphase and SEI layer in the cell with crosslinked $\text{SPE}_{10:1:1-\text{CL}}$, contributing to its good cycling performance. UV-crosslinking appears to play a crucial role in suppressing Li-dendrite formation and facilitating facile and reversible Li plating-stripping.⁴²

3.6 Performance of solid-state LMBs

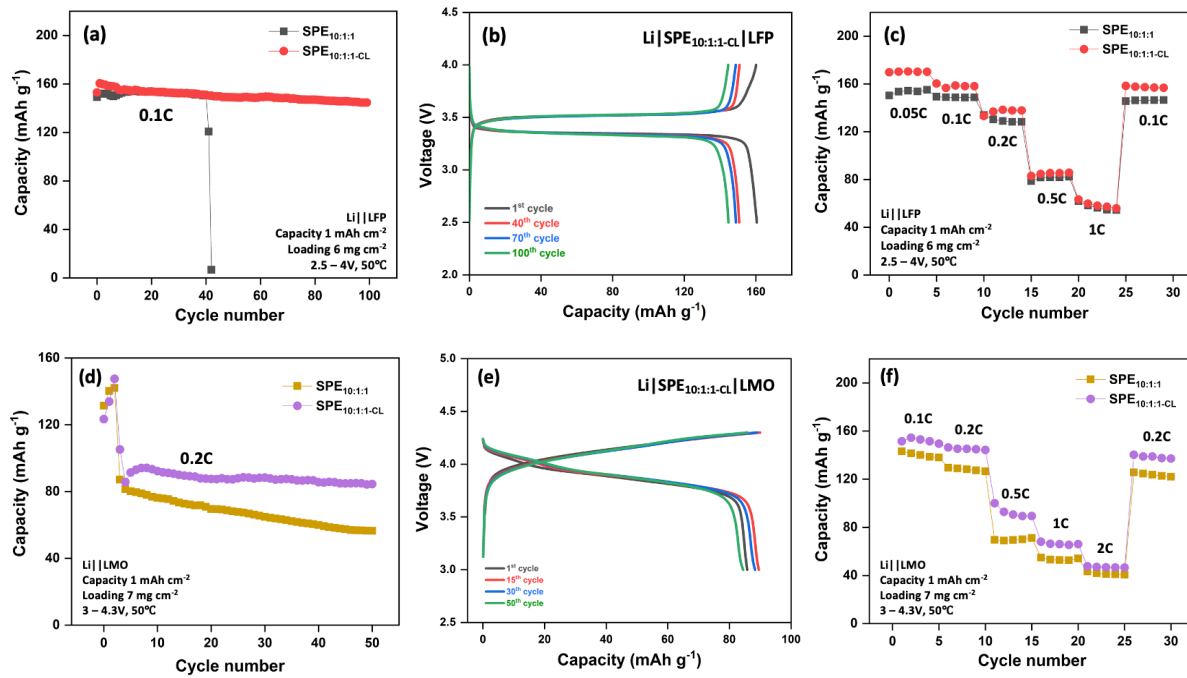


Figure 5. (a) Cycling performance of LFP||Li (active mass loading 6 mg cm^{-2}) cell cycled at 0.1 C rate between 2.5–4.0 V for 100 cycles at 50°C. (b) Charge-discharge profiles of different cycle numbers at 0.1 C rate. (c) Rate performances of LFP||Li cell at different C rates. (d) Cycling performance of LMO||Li (active mass loading 7 mg cm^{-2}) cell cycled at 0.2 C rate between 3–4.3 V for 50 cycles at 50°C. (e) Charge-discharge profiles of different cycle numbers at 0.2 C rate. (f) Rate performances of LMO||Li cell at different C rates.

The prepared SPE_{10:1:1} and SPE_{10:1:1-CL} membranes were first incorporated into high loading (6 mg cm^{-2}) LFP||Li cells to investigate their performance in solid-state LMBs. **Figure 5a** presents the prolonged cycling results for both LFP|SPE_{10:1:1}|Li and LFP|SPE_{10:1:1-CL}|Li cells at 0.1 C (0.05 mA cm^{-2} current density). The LFP|SPE_{10:1:1-CL}|Li cell incorporating a crosslinked membrane exhibits an initial discharge capacity of 160 mAh g^{-1} , maintaining 90% of its capacity after 100 cycles, achieving excellent coulombic efficiency of nearly 99.8% throughout cycling. In contrast, the LFP|SPE_{10:1:1}|Li cell with non-crosslinked membrane exhibits an initial capacity of 158 mAh g^{-1} but experienced a short circuit after 42 cycles. **Figure 5b** shows the charge–discharge profiles of the LFP|SPE_{10:1:1-CL}|Li cell at different cycle numbers, noting that while the discharge capacity decreased, the charge and discharge curves remained very stable over 100 cycles. A rate capability test, detailed in **Figure 5c**, was conducted at current densities of 0.05 to 1 mA cm⁻² (1C equals 1 mA cm^{-2}). Compared to the LFP|SPE_{10:1:1}|Li cells, the LFP|SPE_{10:1:1-CL}|Li cells exhibited improved rate capability, maintaining nearly full capacity at 0.05C. Overall, the battery delivered high discharge capacity ranging from $170\text{--}59 \text{ mAh g}^{-1}$ at 0.05 to 1C. **Figure S6a** presents charge–discharge profiles of the LFP|SPE_{10:1:1-CL}|Li cell at various C-rates within a voltage range of 2.5–4.0 V vs. Li⁺/Li, showing stable potential plateaus and increasing overpotential with higher C rates. AC impedance profiles (**Figure S6b**) showed a steady decrease in interfacial resistance from 0.05C to 0.2C as the crosslinked membrane adapted itself with the electrode, followed by a slight increase at 0.5C and 1C rate due to interface stability. The improved rate performance and cycling stability of the LFP|SPE_{10:1:1-CL}|Li cell demonstrate the advantages of the crosslinked SPE_{10:1:1-CL}, providing superior electrochemical stability at 50°C.

Given the high stability at anodic voltage observed from LSV tests, LMO||Li cells were explored using the crosslinked and non-crosslinked PCIL-SPEs. **Figure 5d** illustrates the cycling performance of both the LMO|SPE_{10:1:1}|Li and LMO|SPE_{10:1:1-CL}|Li cells at 0.2C (0.1 mA cm⁻² current density) in the voltage range of 3–4.3 V vs. Li⁺/Li. The LMO|SPE_{10:1:1-CL}|Li cell showed an initial discharge capacity of 91.4 mAh g⁻¹, maintaining 93% of its capacity after 50 cycles, whereas the LMO|SPE_{10:1:1}|Li cell experienced 25% discharge capacity loss after the same number of cycles. **Figure 5e** presents the corresponding charge–discharge profiles of the LMO|SPE_{10:1:1-CL}|Li cell at different cycle numbers, showing stable and relatively small over potential throughout cycling. To evaluate the effect of crosslinking on fast charge/discharge capability, rate-capability tests were performed and compared across current densities from 0.05 to 1 mA cm⁻² (shown in **Figure 5f**). The LMO|SPE_{10:1:1-CL}|Li cell exhibited full capacity of 152 mAh g⁻¹ at 0.1 mA cm⁻² and a high capacity of 145 mAh g⁻¹ at 0.1 mA cm⁻². The cell maintained 45% and 32% of its capacity at 1 mA cm⁻² and 2 mA cm⁻² (2C), respectively. Upon reducing the current density back to 0.1 mA cm⁻², the capacity was restored to 139 mAh g⁻¹. The voltage profiles of the LMO|SPE_{10:1:1-CL}|Li cell at different C rate are given in **Figure S7**.

Finally, compared with other types of PEO-based SPEs reported in the literature, the promising performances of the developed crosslinked SPE_{10:1:1-CL} are highlighted (as shown in **Table S1**). It not only shows excellent cycling performance with high loading LFP cathodes, but also surprisingly good compatibility with very high loading, high energy 4V-class LMO cathodes, which is a remarkable result within the PEO-based SPE family due to the low oxidative stability of PEO. Our findings collectively highlight the synergistic benefits of concentrated ionic liquid and the crosslinking approach in the designed PCIL-SPEs. The superior rate performance and prolonged cycling stability observed in the crosslinked PCIL-SPEs suggest they are a promising avenue for their deployment in high energy density solid-state LMBs.

4. Conclusion

In this study, we report a newly designed crosslinked PEO-in-concentrated ionic liquid (CIL) SPEs for use in high energy solid-state LMBs. The proper combination of using CIL and UV-crosslinking shows synergistic advantages in reducing PEO crystallinity, increasing ionic conductivity, and enhancing the electrochemical stability of the designed SPEs. These innovations yield crosslinked SPE_{10:1:1-CL} with high ambient temperature ionic conductivity of 4×10^{-4} S cm⁻¹ and a wide electrochemical stability window reaching up to 4.9 V vs. Li⁺/Li. Raman analysis confirms that these promising properties are ascribed to enhanced Li⁺ solvation and increased Li⁺-EO coordination after crosslinking, which significantly enhances SPE oxidation stability. The crosslinked PCIL-SPEs demonstrated stable Li symmetric plating/stripping cycling and remarkable electrochemical performance (almost full capacity, excellent coulombic efficiency, and stable cycling even at high current regimes) with both high loading LFP and, particularly, high energy LMO cathodes, highlighting their strong potential for practical applications in high energy density solid-state LMBs. This study not only advances the development of PEO-based SPEs but also underscores their potential to impact the broader field of sustainable and high-performance energy storage solutions.

Acknowledgements

The authors would like to acknowledge the financial support of the European Union's Horizon 2020 research and innovation programme under the Marie Skłodowska-Curie Grant agreement (Grant No. 860403) and the Australian Research Council for providing funding through the Industry Transformation Training Centre for Future Energy Technologies (storEnergy). Deakin University's Advanced Characterisation Facility is acknowledged for use of the NMR facility. The authors also thank the Battery Technology Research and Innovation Hub (BatTRI-Hub) at Deakin University for their battery prototyping facilities. This study was carried out within the MOST – Sustainable Mobility Center and received funding from the European Union Next-GenerationEU (PIANO NAZIONALE DI RIPRESA E RESILIENZA – PNRR – MISSIONE 4 COMPONENTE 2, INVESTIMENTO 1.4 e D.D. 1033 June 17, 2022, CN00000023). This manuscript reflects only the authors' views and opinions, neither the European Union nor the European Commission can be considered responsible for them.

References

1. Armand, M. Polymer solid electrolytes - an overview. *Solid State Ion.* **9–10**, 745–754 (1983).
2. Fenton, D. E., Parker, J. M. & Wright, P. V. Complexes of alkali metal ions with poly(ethylene oxide). *Polymer* **14**, 589 (1973).
3. Xue, Z., He, D. & Xie, X. Poly(ethylene oxide)-based electrolytes for lithium-ion batteries. *J. Mater. Chem. A* **3**, 19218–19253 (2015).
4. Xiao, S., Ren, L., Liu, W., Zhang, L. & Wang, Q. High-voltage polymer electrolytes: Challenges and progress. *Energy Storage Mater.* **63**, 102970 (2023).
5. Gadjourova, Z., Andreev, Y. G., Tunstall, D. P. & Bruce, P. G. Ionic conductivity in crystalline polymer electrolytes. *Nature* **412**, 520–523 (2001).
6. Chen, L. *et al.* PEO/garnet composite electrolytes for solid-state lithium batteries: From “ceramic-in-polymer” to “polymer-in-ceramic”. *Nano Energy* **46**, 176–184 (2018).
7. Song, X. *et al.* Unraveling the Synergistic Coupling Mechanism of Li⁺ Transport in an “Ionogel-in-Ceramic” Hybrid Solid Electrolyte for Rechargeable Lithium Metal Battery. *Adv. Funct. Mater.* **32**, 2108706 (2022).

8. Zhang, X. *et al.* Vertically Aligned and Continuous Nanoscale Ceramic–Polymer Interfaces in Composite Solid Polymer Electrolytes for Enhanced Ionic Conductivity. *Nano Lett.* **18**, 3829–3838 (2018).
9. Porcarelli, L., Gerbaldi, C., Bella, F. & Nair, J. R. Super Soft All-Ethylene Oxide Polymer Electrolyte for Safe All-Solid Lithium Batteries. *Sci. Rep.* **6**, 19892 (2016).
10. Kim, G. T. *et al.* UV cross-linked, lithium-conducting ternary polymer electrolytes containing ionic liquids. *J. Power Sources* **195**, 6130–6137 (2010).
11. Armand, M., Endres, F., MacFarlane, D. R., Ohno, H. & Scrosati, B. Ionic-liquid materials for the electrochemical challenges of the future. *Nat. Mater.* **8**, 621–629 (2009).
12. Shin, J. Ionic liquids to the rescue? Overcoming the ionic conductivity limitations of polymer electrolytes. *Electrochem. Commun.* **5**, 1016–1020 (2003).
13. Falco, M. *et al.* Understanding the Effect of UV-Induced Cross-Linking on the Physicochemical Properties of Highly Performing PEO/LiTFSI-Based Polymer Electrolytes. *Langmuir* *acs.langmuir.9b00041* (2019) doi:10.1021/acs.langmuir.9b00041.
14. Watanabe, M., Nagano, S., Sanui, K. & Ogata, N. Ionic Conductivity of Network Polymers from Poly(ethylene oxide) Containing Lithium Perchlorate. *Polym. J.* **18**, 809–817 (1986).
15. Joost, M. *et al.* Ionic mobility in ternary polymer electrolytes for lithium-ion batteries. *Electrochimica Acta* **86**, 330–338 (2012).
16. Gerbaldi, C. *et al.* UV-cured polymer electrolytes encompassing hydrophobic room temperature ionic liquid for lithium batteries. *J. Power Sources* **195**, 1706–1713 (2010).
17. Nair, J. R. *et al.* UV-cured methacrylic membranes as novel gel–polymer electrolyte for Li-ion batteries. *J. Power Sources* **178**, 751–757 (2008).

18. Yoshida, K. *et al.* Oxidative-Stability Enhancement and Charge Transport Mechanism in Glyme–Lithium Salt Equimolar Complexes. *J. Am. Chem. Soc.* **133**, 13121–13129 (2011).
19. Wang, J. *et al.* Superconcentrated electrolytes for a high-voltage lithium-ion battery. *Nat. Commun.* **7**, 12032 (2016).
20. Suo, L. *et al.* “Water-in-salt” electrolyte enables high-voltage aqueous lithium-ion chemistries. *Science* **350**, 938–943 (2015).
21. Gao, X., Wu, F., Mariani, A. & Passerini, S. Concentrated Ionic-Liquid-Based Electrolytes for High-Voltage Lithium Batteries with Improved Performance at Room Temperature. *ChemSusChem* **12**, 4185–4193 (2019).
22. Chen, F., Howlett, P. & Forsyth, M. Na-Ion Solvation and High Transference Number in Superconcentrated Ionic Liquid Electrolytes: A Theoretical Approach. *J. Phys. Chem. C* **122**, 105–114 (2018).
23. Chen, C.-Y. *et al.* Ionic liquid electrolytes with high sodium ion fraction for high-rate and long-life sodium secondary batteries. *J. Power Sources* **332**, 51–59 (2016).
24. Giffin, G. A., Moretti, A., Jeong, S. & Passerini, S. Decoupling effective Li⁺ ion conductivity from electrolyte viscosity for improved room-temperature cell performance. *J. Power Sources* **342**, 335–341 (2017).
25. Pal, U. *et al.* Enhanced ion transport in an ether aided super concentrated ionic liquid electrolyte for long-life practical lithium metal battery applications. *J. Mater. Chem. A* **8**, 18826–18839 (2020).
26. Pal, U. *et al.* Improved Li-Ion Transport by DME Chelation in a Novel Ionic Liquid-Based Hybrid Electrolyte for Li–S Battery Application. *J. Phys. Chem. C* **122**, 14373–14382 (2018).

27. Pal, U. *et al.* Interphase control for high performance lithium metal batteries using ether aided ionic liquid electrolyte. *Energy Environ. Sci.* **15**, 1907–1919 (2022).
28. Pal, U. *et al.* A High-Performing Spinel LiMn₂O₄ Cathode Material with Unique Morphology and Scaled Manufacture. <https://chemrxiv.org/engage/chemrxiv/article-details/65608db3cf8b3c3cd704658b> (2023) doi:10.26434/chemrxiv-2023-1z161.
29. He, R. & Kyu, T. Effect of Plasticization on Ionic Conductivity Enhancement in Relation to Glass Transition Temperature of Crosslinked Polymer Electrolyte Membranes. *Macromolecules* **49**, 5637–5648 (2016).
30. Zhang, M. *et al.* Advanced High-Voltage Electrolyte Design Using Poly(ethylene oxide) and High-Concentration Ionic Liquids for All-Solid-State Lithium Metal Batteries. Preprint at <https://doi.org/10.26434/chemrxiv-2024-5sqth> (2024).
31. Al-Masri, D., Yunis, R., Hollenkamp, A. F. & Pringle, J. M. Designing Solid-State Electrolytes through the Structural Modification of a High-Performing Ionic Liquid. *ChemElectroChem* **7**, 4118–4123 (2020).
32. Jin, L. *et al.* Structure and Transport Properties of a Plastic Crystal Ion Conductor: Diethyl(methyl)(isobutyl)phosphonium Hexafluorophosphate. *J. Am. Chem. Soc.* **134**, 9688–9697 (2012).
33. Susan, Md. A. B. H., Kaneko, T., Noda, A. & Watanabe, M. Ion Gels Prepared by in Situ Radical Polymerization of Vinyl Monomers in an Ionic Liquid and Their Characterization as Polymer Electrolytes. *J. Am. Chem. Soc.* **127**, 4976–4983 (2005).
34. Joost, M., Kim, G. T., Winter, M. & Passerini, S. Phase stability of Li-ion conductive, ternary solid polymer electrolytes. *Electrochimica Acta* **113**, 181–185 (2013).
35. Berthier, C., Gorecki, W. & Minier, M. MICROSCOPIC INVESTIGATION OF IONIC CONDUCTIVITY IN ALKALI METAL SALTS-POLY(ETHYLENE OXIDE) ADDUCIS.

36. Stettner, T., Lingua, G., Falco, M., Balducci, A. & Gerbaldi, C. Protic Ionic Liquids-Based Crosslinked Polymer Electrolytes: A New Class of Solid Electrolytes for Energy Storage Devices. *Energy Technol.* **8**, 2000742 (2020).
37. Kimura, K., Motomatsu, J. & Tominaga, Y. Correlation between Solvation Structure and Ion-Conductive Behavior of Concentrated Poly(ethylene carbonate)-Based Electrolytes. *J. Phys. Chem. C* **120**, 12385–12391 (2016).
38. Nguyen, H. T. T. *et al.* Facile Li⁺ Transport in Interpenetrating O- and F-Containing Polymer Networks for Solid-State Lithium Batteries. *Adv. Funct. Mater.* **33**, 2213469 (2023).
39. Wu, H. *et al.* A Polymer-in-Salt Electrolyte with Enhanced Oxidative Stability for Lithium Metal Polymer Batteries. *ACS Appl. Mater. Interfaces* **13**, 31583–31593 (2021).
40. Xu, K., Ding, S. P. & Jow, T. R. Toward Reliable Values of Electrochemical Stability Limits for Electrolytes. *J. Electrochem. Soc.* **146**, 4172–4178 (1999).
41. Herbers, L. *et al.* The Influence of Polyethylene Oxide Degradation in Polymer-Based Electrolytes for NMC and Lithium Metal Batteries. *Adv. Energy Sustain. Res.* **4**, 2300153 (2023).
42. Porcarelli, L., Gerbaldi, C., Bella, F. & Nair, J. R. Super Soft All-Ethylene Oxide Polymer Electrolyte for Safe All-Solid Lithium Batteries. *Sci. Rep.* **6**, 19892 (2016).